

# Extinction Columns and Intrinsic X-ray Spectra of the Anomalous X-ray Pulsars

Martin Durant and Marten H. van Kerkwijk

*Department of Astronomy and Astrophysics, University of Toronto  
60 St. George St, Toronto, ON  
M5S 3H8, Canada*

## ABSTRACT

The X-ray spectra of Anomalous X-ray Pulsars have long been fit by smooth, empirical models such as the sum of a black-body plus a power law. These reproduce the  $\sim 0.5$  to  $10$  keV range well, but fail at lower and higher energies, grossly over-predicting the optical and under-predicting the hard X-ray emission. A poorly constrained source of uncertainty in determining the true, intrinsic spectra, in particular at lower energies, is the amount of interstellar extinction. In previous studies, extinction column densities with small statistical errors were derived as part of the fits of the spectra to simple continuum models. Different choices of model, however, each produced statistically acceptable fits, but a wide range of columns. Here, we attempt to measure the interstellar extinction in a model-independent way, using individual absorption edges of the elements O, Fe, Ne, Mg and Si in X-ray grating spectra taken with *XMM-Newton*. We find that our inferred equivalent hydrogen column density  $N_{\text{H}}$  for 4U 0142+61 is a factor of 1.4 lower than the typically quoted value from black-body plus power-law fits, and is now consistent with estimates based on the dust scattering halo and visual extinction. For three other sources, we find column densities consistent with earlier estimates. We use our measurements to recover the intrinsic spectra of the AXPs empirically, without making assumptions on what the intrinsic spectral shapes ought to be. We find that the power-law components that dominate at higher energies do not extend below the thermal peak.

*Subject headings:* pulsars: anomalous X-ray pulsars, X-ray spectroscopy, ISM, pulsars: individual (4U 0142+61, 1E 2259+586, 1E 1048.1–5937, 1RXS J170849.0–400910)

## 1. Introduction

The Anomalous X-ray Pulsars (AXPs) are a group of about six young, isolated neutron stars showing pulsations with periods of the order 10 s, whose high-energy luminosity vastly

exceeds what is available in rotational energy losses. They are modeled as *magnetars*, their energetics dominated by energy released from a decaying super-strong magnetic field,  $\sim 10^{14}$  G externally. See Woods & Thompson (2004) for a summary of current observations and their interpretation in the context of the magnetar model.

Since their discovery, the X-ray spectra of the AXPs have been fitted with simple continuum models, most commonly the sum of a black body, representing the peak of the spectrum around a few keV, and a power law to account for the emission at higher energies. The overall spectra are relatively soft, as indicated by high power-law indices. In the fitting process, the interstellar extinction is estimated as well, by including a multiplicative term to take account of the absorption of all elements, parameterized by the hydrogen column density,  $N_{\text{H}}$ .

While these smooth continuum spectral models reproduce the spectra of all AXP well in the range observed by satellites such as *Chandra*, *XMM* and *ASCA* (roughly 0.5 to 10 keV), their extrapolation fails at both higher and lower energies. At energies from tens of keV to  $\sim 1$  MeV, Kuiper et al. (2004) and Den Hartog (2006) found from RXTE/HEXE and Integral observations that much harder power-law components are present, which dominate the total energetics. In the optical and infrared, the first detections of AXPs made by Hulleman et al. (2000, 2001) already showed that while the optical and infrared emission is only a tiny part of the energy budget, it is well below (by orders of magnitude) the extrapolation of the X-ray spectra dominated by the power law, yet well above the extrapolation of just a blackbody component. Thus, the optical and infrared emission also appears to require a separate emission component. More recently, the situation was complicated even further, when Wang et al. (2006) found from mid-infrared observations from *Spitzer* that at least one of the AXPs (4U 0142+61) shows evidence of a circumstellar dusty disc.

The above discrepancies led us to wonder whether the measurements of interstellar extinction were reliable. These are particularly sensitive to the the low-energy ( $< 500$  eV) part of the spectra (where the absorption is highest), and one would expect that they would depend strongly on the assumed model for the intrinsic emission. For instance, the above-mentioned model consisting of a black-body and a power-law component rises towards lower energies, while a model of, say, two black-body components, would turn over. Thus, to match a given observation, the former would require a larger column density than the latter.

From previous studies (see Table 1), it is indeed clear that the inferred column density  $N_{\text{H}}$  depends strongly on the assumed intrinsic model, with the differences in  $N_{\text{H}}$  for different models fitted to the same spectrum far exceeding the statistical uncertainty obtained for any given one. Clearly, without knowing the intrinsic shape of the spectrum, one cannot measure the extinction accurately, and, conversely, without knowing the extinction independently, one

can obtain only little information about the true intrinsic spectrum.

Another clue that the extinction is not estimated correctly, and hence that the models used for the intrinsic spectrum are incorrect, comes from variability studies. AXP spectra have been seen to vary both from one epoch to another, and between phase bins (e.g., Woods et al. 2004; Rea et al. 2005), and, generally, different values of  $N_{\text{H}}$  are found for these different spectra (see Table 1). Although an intrinsic, variable contribution to the extinction is not impossible in light of the discovery of a possible debris disk around 4U 0142+61 (Wang et al. 2006), it seems unlikely, especially on the time-scale of seconds. Indeed, discrepancies in fitted parameters obtained from spectra taken with different instruments, which are often blamed on poor cross-calibration, could well be purely an artifact of the fitting process, with differences in sensitivities leading to differences in weight as a function of energy, and hence different values for the parameters, including the extinction.<sup>1</sup>

From a physical perspective, it is not clear why there should be a power-law component in the spectra of AXPs. Recent physical models, such as those presented by Lyutikov & Gavriil (2006) can account for a power-law like high-energy tail, but do not predict a soft part. In these models, the blackbody surface flux is modified by interactions in the outer atmosphere or magnetosphere, for example through the inverse-Compton scattering of photons off high-energy particles. This creates an extended high-energy tail but leaves the spectrum at low energies (the Rayleigh-Jeans side of the blackbody spectrum) unaffected.

Absorption in the interstellar medium of X-ray photons is primarily by the photo-electric capture by electrons in inner shells of metals and helium. Since the creation of X-ray absorption models (Morrison & McCammon 1983; Balucinska-Church & McCammon 1992), great advances have been made in our understanding of absorption edge structure and energies (e.g., Juett et al. 2003), largely driven by the improved resolution and sensitivity of X-ray observatories. We are also beginning to understand more about interstellar abundances (e.g., Lodders 2003; but see §5 below). With these advances, it is now possible to measure individual elemental absorbing columns to a source independently, and so recover the intrinsic spectrum without further assumptions.

In this paper, we measure the extinction to the four best-studied AXPs by analyzing the individual absorption edges present in the sensitivity range of XMM/RGS, and use this to derive intrinsic X-ray spectra for each AXP, as well as to estimate reddening at optical and infrared wavelengths. In §2, we present the data sets we use and their reduction. We describe in §3 how we infer individual element column densities, and what atomic data we use. In

---

<sup>1</sup>Another source of differences may be the use of different sets of cross-sections and abundances; see, e.g., Weisskopf et al. (2004).

Table 1. Hydrogen column densities towards the AXPs inferred using different models.

Object	Telescope/ instrument	Model <sup>a</sup>					Reference
		PL	PL+BB	BB+BB	BR	BR+BB	
4U 0142+61	XMM/EPIC	...	0.96	...	0.82	0.68	Göhler et al. (2004)
	Chandra/HETGS	1.43:	0.88	...	0.92	0.69	Juett et al. (2002)
	ASCA/SIS, GIS	...	0.95	...	...	0.90	White et al. (1996)
1E 2259+586	XMM/EPIC	...	0.94-1.10 <sup>b</sup>	...	...	...	Woods et al. (2004)
	Chandra/ACIS	...	0.93	...	...	...	Patel et al. (2001)
	ASCA/PSPC	1.14:	0.85	0.63	0.8	...	Rho & Petre (1997)
1E 1048.1-5937	XMM/EPIC	...	0.95-1.10 <sup>b</sup>	0.55-0.67 <sup>b</sup>	...	...	Tiengo et al. (2005)
	BeppoSAX/LECS	1.54:	0.45	0.14	...	...	Oosterbroek et al. (1998)
1RXS J170849.0 -400910	BeppoSAX/LECS	...	1.3-1.7 <sup>c</sup>	...	...	...	Rea et al. (2005)
	BeppoSAX/LECS	...	1.1-1.6 <sup>c</sup>	...	...	...	Rea et al. (2003)

Note. — Column Densities are in units ( $10^{22} \text{ cm}^{-2}$ ). For all models listed, the reduced  $\chi^2$  of the fits was less than 2 (those marked with colons are relatively poor fits).

<sup>a</sup>Acronyms are PL: Power Law, BB: Black Body, BR: Bremsstahlung.

<sup>b</sup>Ranges represent measurements made at different epochs. One does not expect the column density to vary with time (see text).

<sup>c</sup>Range represents measurements in different phase bins. Again, one would not expect the column density to vary with rotational phase.

§4, we use Monte-Carlo simulations to estimate the uncertainties of our measurements. We present our results in §5, and show de-extincted X-ray spectra in §6. We continue by deriving optical extinctions for all sources in §7, and discussing the overall spectral energy distribution of the best-studied source, 4U 0142+61, in §8. We briefly summarize our results and look forward to future work in §9.

## 2. Data Reduction

We searched the *XMM-Newton* archive for observations of all the AXPs. The *XMM-Newton* observatory (Jensen, 1999) provides data from three separate telescopes simultaneously, but in this work we are concerned with the Reflection Grating Spectrometer (RGS) instruments (den Herder et al. 2001), which provide high-resolution spectra in the range 6–40 Å. We found a number of long observations for the four brightest AXPs<sup>2</sup> (see Table 2; we omitted shorter data sets with few counts). For all these, RGS is used with the same instrumental setup, thus ensuring a fair comparison of the sources. We also searched for high-resolution spectra taken by *Chandra*, but found only a few observations. Since these did not allow a comparison between sources, we decided not to use these in the present work.

We reduced the raw data (Observation Data Files or ODFs) with the 20041122 version of the analysis software, XMM-SAS, and calibration files. We used the pipeline products for the data from the European Photon Imaging Cameras, EPIC (Strüder et al. 2001; Turner et al. 2001; these were used only as additional information for the RGS reduction, see below).

A light curve was produced with 10-s bins from the EPIC data. These showed periods of high background (*flaring*), and such periods were excised from the RGS analysis using Good Time Intervals (GTIs). The EPIC data was also used for source selection, using the automated source detection algorithm. This only works for imaging modes, but fortunately there are three imaging instruments (EMOS1, EMOS2, EPN), and out of these only one is required. The co-ordinates of the brightest source were used to extract the RGS spectra. This eliminates any uncertainties arising from the telescope pointing and bore-sight correction, since the relative alignment of the telescopes and instruments is well known.

Final spectra were obtained by subtracting the background and then converting to flux using the XMM-SAS task `rgsfluxer`. For our spectral modeling, we decided to bin to a relatively low resolution (0.1 Å), since the errors associated with bins with few or no counts is

---

<sup>2</sup>For the AXP 1E 1841-045, two short XMM observations exist, but we found these contained too few counts to provide reliable measurements.

uncertain. We kept a large number of bins in the spectra and response matrix functions until the final fluxing, as recommended in the documentation. The documentation also states that `rgsfluxer` fluxes are not recommended for final scientific analysis, but for the relatively low resolution we use and the relatively poor signal-to-noise ratio of our data, the accuracy is ample.

In order to improve the signal-to-noise ratio, we decided to merge the spectra from different observations of each object into averaged spectra. Here, we must raise two caveats. The first is that some AXPs – 1E 1048.1–5937 in particular – are variable, and the spectral shape may be different in each observation. This, however, should not change our column estimates, since we fit in small spectral regions around each absorption edge. The second caveat is that the amount of extinction to the continuum source might vary if some of it is intrinsic. This seems unlikely, but is perhaps not impossible given the discovery by Wang et al. (2006) of a likely debris disc around 4U 0142+61 (although from broad-band observations there has been no clear evidence for changes in extinction). Unfortunately, our individual datasets do not have enough signal to verify this.

Finally, we note that for 1E 2259+586 there is enhanced background emission due to the supernova remnant surrounding the AXP. From the pipeline-produced *order images*, however, we find that the spectrum of the central source remains distinguishable and that there are no significant background lines which might contaminate it. The increased background does, however, lead to poorer signal-to-noise where the AXP flux is low.

### 3. Analysis

For our measurements, we assume that it is possible to find small regions of a spectrum around an absorption edge, over which the intrinsic spectrum is continuous and well-described by a power-law. To each spectral region of interest, we fit a function of the form

$$F_\lambda = A \times \left( \frac{\lambda}{\lambda_{\text{edge}}} \right)^\alpha \times \begin{cases} 1 & \text{for } \lambda > \lambda_{\text{edge}} \\ \exp \left[ - \left( \frac{\lambda}{\lambda_{\text{edge}}} \right)^{5/2} \times N\sigma \right] & \text{for } \lambda \leq \lambda_{\text{edge}} \end{cases} \quad (1)$$

In the fits, the edge wavelength  $\lambda_{\text{edge}}$  and photo-ionization cross-section at the edge  $\sigma$  were kept fixed, but the normalization  $A$ , power-law index  $\alpha$  and the column density  $N$  were allowed to vary. Note that the value of the power-law index which attenuates the cross-section with wavelength here is not the more familiar 3. The value of 2.5 fits better with theoretical calculations (e.g., Verner & Yakovlev 1995). We note that the fits below are insensitive to this change, and negligible additional uncertainty is incurred.

Table 2. Data sets used.

Object	Dataset <sup>a</sup>	Date	Exp. <sup>b</sup> (ks)	Counts <sup>c</sup> (1000)
4U 0142+61	0206670101	2004-03-01	44.1	98.5
	0206670201	2004-07-25	23.9	62.6
1E 2259+586	0038140101	2002-06-11	52.5	20.2
	0155350301	2002-06-21	29.0	22.8
1E 1048.1–5937	0147860101	2003-06-16	69.0	2.3
	0164570301	2004-07-08	33.9	4.6
	0307410201	2005-06-16	23.3	3.4
	0307410301	2005-06-28	25.9	2.6
1RXS J170849.0–400910	0148690101	2003-08-28	44.9	11.2

<sup>a</sup>XMM Science Archive identifier

<sup>b</sup>Exposure time for the RGS instruments only; typically shorter than the total observation time.

<sup>c</sup>In both RGS instruments, in two orders, after good-time-interval filtering and background subtraction.

We used theoretical photo-electric cross-sections from Gould & Jung (1991), since cross-sections are very hard to measure accurately. From recent high-resolution X-ray spectroscopy (see below), we know of several narrow features and additional structure in some of the edges. In contrast to the overall strength of the ionisation edges, the strengths of these additional features depend on the degree of ionisation along the line of sight. Since we do not have enough signal to fit for these, we instead mask any affected points. The spectral ranges to fit around each edge were chosen by balancing the requirement of enough data points for robust fits with that of the intrinsic spectra being well described by power-law form.

For the Oxygen-K edge ( $\sigma = 5.642 \times 10^{-19} \text{ cm}^{-2}$ ), we fitted the range 19–26 Å and used  $\lambda_{\text{edge}} = 23.1 \text{ \AA}$ , as found by Takei et al. (2002). We masked the regions 22.5–23.1 Å for multiple edges, and 23.25–23.6 Å for narrow lines.

For the Iron-L edge(s) ( $\sigma = 4.936 \times 10^{-19} \text{ cm}^{-2}$ ), we fitted the 16–19 Å range and used an edge wavelength of 17.52 Å, following the work of Juett et al. (2006, in prep.). There are no sharp absorption features, but the edge has multiple components, leading to a complex shape around the edge. Accordingly, we masked the range 17.2–17.56 Å.

In the case of the Neon-K edge ( $\sigma = 3.523 \times 10^{-19} \text{ cm}^{-2}$ ), we fitted the range 13–16 Å and used  $\lambda_{\text{edge}} = 14.31 \text{ \AA}$  following once more the work of Juett et al. Three narrow absorption features fall into the fitting range, which we excluded by masking 14.44–14.66 Å and 13.4–13.5 Å.

The Magnesium-K edge ( $\sigma = 2.191 \times 10^{-19} \text{ cm}^{-2}$ ) is the only one in our sample which shows no complicated features. We used  $\lambda_{\text{edge}} = 9.5 \text{ \AA}$ , as found by Ueda et al. (2005), and fitted in the range 8.5–10.5 Å.

Finally, for the Silicon-K edge ( $\sigma = 1.476 \times 10^{-19} \text{ cm}^{-2}$ ), we once more used the work of Ueda et al., fitting in the range 6.2–7.5 Å and using  $\lambda_{\text{edge}} = 6.72 \text{ \AA}$ . We masked the region 6.61–6.73 Å for edges of silicon in silicates, which are slightly shifted from the edge for atoms in isolation.

#### 4. Fitting Method and Error Determination

For each edge, we fit the data with the model in Eq. 1, with  $\lambda_{\text{edge}}$  and  $\sigma$  fixed to the values given above, and the best values of  $A$ ,  $\alpha$ , and  $N$  found by  $\chi^2$  minimization. For the uncertainties on each data point, we use the errors given by `rgsfluxer`.

There are two possible problems with our fitting method. First, the uncertainties produced by `rgsfluxer` are known to be poorly defined for faint sources. This is because in the

high-resolution input spectra (which are rebinned to our  $0.1\text{\AA}$  bin size in `rgsfluxer`), bins with zero counts are assigned an arbitrary uncertainty of 1, when the expectation value for the (faint) source might genuinely be near zero and hence the associated uncertainty should be smaller as well. These assigned errors are propagated, and, as a result, the uncertainties on the rebinned fluxes are greatly overestimated, leading to values of reduced  $\chi^2$  far smaller than unity in our fits. The second possible problem, related to this, is that for these counting data, it would be more appropriate to use the Cash statistic rather than  $\chi^2$ , since the probability distribution is Poissonian rather than Gaussian.

Fortunately, in practice these problems are not severe. In a given fitting region, we find that in our  $0.1\text{\AA}$  bins both the number of counts and the `rgsfluxer` uncertainty are roughly constant. Thus, even though the given errors are over-estimated, this effect is roughly equal for each point and hence it does not effect the best-fit parameters. Furthermore, the bins we use are sufficiently wide that they contain many counts, and hence the assumption of Gaussian uncertainties is not so bad. Indeed, fits made by minimizing the Cash statistic led to results very close to those found through the  $\chi^2$  method. We preferred not to use them generally, however, since with the Cash minimization our fitting routine converged much less robustly to the global best fit.

In order to estimate the uncertainties on our measurements, we have conducted Monte-Carlo simulations, in which we produce simulated data sets which we fit in the same manner as the real data. We employed two different methods for simulating the data. In the first, we used *bootstrapping*, i.e., we produced simulated data sets with the same number of points as the actual data set by drawing randomly, with replacement, from the actual  $(\lambda, F_\lambda)$  pairs (Press et al. 1992). In the second method, we simulated data sets based on the best-fit model, adding Gaussian noise with a variance equal to the variance of the real data around that model. Both methods gave consistent results after 1000 trials and the spread of results in the one parameter of interest (the column depth), was well-described by a Gaussian in every case. The one-sigma confidence region was taken to be the region enclosed by the 16th and 84th percentile and these are listed in Table 3.

We note that in some cases, in particular for 1E 1048.1–5937, the uncertainties even for the best measurements are similar to the measurements themselves, i.e., the measurements of the individual columns are not significant. In evaluating this, however, one should keep in mind that we know *a priori* the locations and shapes of the absorption edges (from high signal-to-noise measurements of brighter sources; see §3). Being in the Galactic plane, interstellar extinction is inevitable, and our aim is not to prove the existence of the features, but just to measure the strength of features known to be present. Thus, the measured column densities and associated uncertainties can be used as given, and, in particular, columns from different

elements can be combined to give a more significant overall measurement of the extinction.

Finally, possible sources of systematic error ought to be mentioned. First, we have chosen to fit the spectral sections with a power law. This should not be a large source of additional uncertainty, since our wavelength ranges are so small –  $\Delta\lambda/\lambda = 0.2 \dots 0.3$  – that a power law should be a good approximation for any smooth continuum. Indeed, the fit would be much better constrained if we could use larger wavelength range, but this would require knowledge of what the intrinsic spectrum ought to be. Second, the optical depth in an edge does not in general have the simplistic form given in Equation 1 – the form is different for every ionisation stage of every element. Fortunately, the equivalent width of the resulting feature – and thus the total column – is not sensitive to such details, since it depends on the total cross section. Third, the masking of certain wavelengths due to complicated near-edge structure is not necessarily the best approach, but the alternative – fitting for them – would not be better, since the details of the strengths of the lines depends upon the (unknown) ionization balance along the line of sight; hence, any gain in number of data points included in the fit would be offset by the required additional parameters.

## 5. Results

In Table 3, we list the inferred columns for each object, and in Figure 1, we show the fits overlaid on the data points, for those objects where a reasonable fit was possible. Note that while points with zero or negative flux were included in the fit, they do not show up in the figures (since the scales are logarithmic).

From the figures and the table, one sees that the values for iron and silicon are in every case uncertain, due to the low flux and low optical depth for the former and the low sensitivity and relatively poor calibration of the RGS at short wavelengths for the latter. Since they do not add information, we will not use these results any further.

For Neon and Magnesium, we find fair measurements for all sources, and one sees that their relative abundances are roughly consistent from one source to another. 1RXS J170849.0–400910 appears to be an exception to this, its magnesium to neon ratio being relatively high, but with the large uncertainties for this highly reddened source, they are still consistent within the errors. From the columns given, it is immediately clear that 4U 0142+61 is least extinguished, followed by 1E 1048.1–5937, 1E 2259+586 and 1RXS J170849.0–400910.

We list in Table 4 the implied Hydrogen column densities for each source, for each reliably measured photo-electric edge. Here, we use the abundances of Asplund et al. (2004); we discuss this further below. Also listed are the weighted means of the column densities.

Table 3. Column densities found for each AXP

AXP	O K ( $10^{17} \text{ cm}^{-2}$ )	Fe L <sup>a</sup> ( $10^{17} \text{ cm}^{-2}$ )	Ne K ( $10^{17} \text{ cm}^{-2}$ )	Mg K ( $10^{17} \text{ cm}^{-2}$ )	Si K <sup>a</sup> ( $10^{17} \text{ cm}^{-2}$ )
4U 0142+61	$28.8 \pm 4.5$	$0.7 \pm 1.4$	$5.3 \pm 1.3$	$2.2 \pm 0.5$	$2.0 \pm 2.7$
1E 2259+586	...	$13 \pm 6$	$9 \pm 4$	$3.6 \pm 1.4$	$0.6 \pm 3.6$
1E 1048.1–5937	...	...	$7 \pm 7$	$2.7 \pm 2.4$	$11 \pm 7$
1RXS J170849.0–400910	...	...	$15 \pm 5$	$2.9 \pm 1.8$	$2 \pm 5$

Note. — No value is shown in cases where no reliable fit was possible.

<sup>a</sup>We list the results for Fe L and Si K for completeness only. As discussed in the §4, we believe these are less reliable.

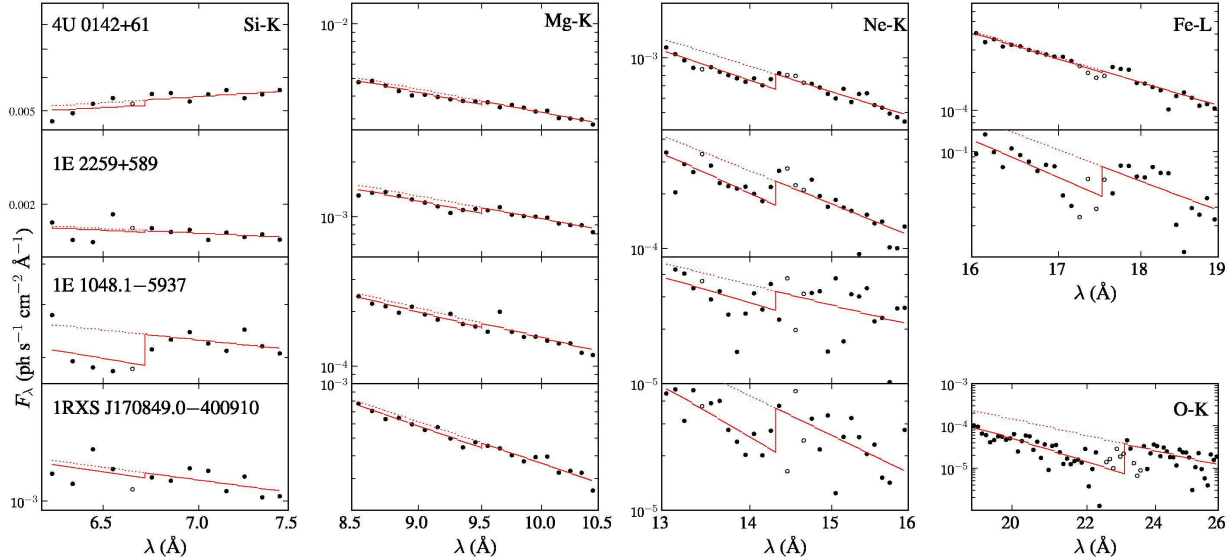


Fig. 1.— Fits obtained for the Si-K, Mg-K, Ne-K and Fe-L edges (left to right), with the O-K edge for 4U 0142+61 only in the lower-right. Open circles have been excluded from the fit, due to complex edge structures or narrow features. For each edge, the scales span the same factor in flux for the different AXPs. As discussed in the §4, we do not use iron or silicon in determining the average extinction, since these results are less reliable.

Comparing our results with those found through broad-band fits using assumed intrinsic models (Table 1), one sees that the values are consistent with the ranges found previously. Unfortunately, for all sources but 4U 0142+61, our uncertainties are too large to distinguish between different models. For 4U 0142+61, however, our value of  $N_{\text{H}}$  is well determined, and we find it to be lower by a factor 1.4 than the value inferred from the commonly used black-body plus power-law model, and closer to that found using the model consisting of two black bodies. Interestingly, this is also the source for which White et al. (1996) found a discrepancy between the extinction and the brightness of its X-ray scattering halo, while Hulleman et al. (2004) found a discrepancy between X-ray extinction, as inferred from the black-body plus power-law model, and optical reddening. With our new value, the different measurements are all consistent.

In the sections below, we will use our  $N_{\text{H}}$  values to derive intrinsic spectra and optical extinctions. Before doing so, it is worth stressing that while we quote values of  $N_{\text{H}}$ , our measurements are of the Neon and Magnesium (and Oxygen for 4U 0142+61) column densities. Thus, the accuracy with which we can determine columns of a given other element (or dust) depends not only on our statistical uncertainty, but also on the uncertainty on the abundance of that element relative to Neon and Magnesium (as well as on possible corrections for the extent to which a given element is locked up in optically thick dust; e.g., Wilms et al. [2000]; for a general caution on the implications of the set of abundances used, see Weisskopf et al. [2004]).

In general, the relative abundances of refractive elements are known precisely from studies of meteorites, but those of the volatiles are much more uncertain, as has recently become apparent again from the controversy on the abundances of Oxygen and Neon. Briefly, Asplund et al. (2004) inferred from improved models for the solar atmosphere that the solar Oxygen and Carbon abundances were much lower than thought previously. The revised abundances, however, led to discrepancies between helioseismology and models for the solar interior (e.g., Schmeltz et al. 2005). To remedy this, it has been suggested that the abundance of Neon might have to be revised upwards (e.g., Bahcall et al. 2005), but this leads to a number of other problems (e.g., Young 2005; Drake & Testa 2005).

From our data, an increased Neon abundance seems unlikely: the value of the Neon to Magnesium ratio we find,  $\text{Ne/Mg} = 2.4 \pm 0.7$ , is much closer to the solar-abundance value of 2.0 from Asplund et al. (2004) than the value of 5.8 hypothesised by Bahcall et al. (2005) for consistency with helioseismology. For Oxygen, we have only one measurement, for 4U 0142+61, which gives  $\text{O/Mg} = 13.1 \pm 3.6$ . This is also much closer to the revised solar abundance of 13.5 of Asplund et al. (2004) than the old one of 22.4 listed by Anders &

Grevesse (1989).<sup>3</sup>

Given the above, we are fairly confident that for columns of other refractive elements (or of dust), any additional uncertainty beyond the statistical one is small. However, we are less confident for the abundances of Hydrogen, Helium, Carbon, Nitrogen, and Oxygen. This will affect our corrections for extinction below, especially at low energies.

## 6. Intrinsic Spectra

The main question underlying this work is the nature of the intrinsic spectra of AXPs. As discussed in §1, different simple models reproduce the spectral data equally well, and they do not allow one, e.g., to distinguish between spectra that rise or fall with decreasing energy at low energies. With the column densities obtained above, we can de-extinct the observations to find the intrinsic spectra empirically. For this purpose, rather than attempt to model the extinction in detail (e.g., Wilms et al. 2000), we will use a simplified model that can be described and reproduced easily; this will be sufficient to answer the main question, whether the intrinsic spectra rise or fall at long wavelengths.

For the extinction correction, we convert the average Hydrogen column densities  $\langle N_{\text{H}} \rangle$  from Table 4 to individual columns for Oxygen, Iron, Neon, Magnesium, and Silicon (using the abundances of Asplund et al. [2004]; see Table 4 for O, Ne, Mg; furthermore,  $N_{\text{Fe}} = 2.8 \times 10^{-5} N_{\text{H}}$ ,  $N_{\text{Si}} = 3.2 \times 10^{-5} N_{\text{H}}$ ), and correct the spectra for the contribution of each of these using the simple edge model from Eq. 1 and the cross sections given following that equation. Furthermore, we take into account the absorption by lighter elements, in particular Helium, Carbon, and Nitrogen, with an additional component  $\exp[-\tau_{25}(\lambda/25 \text{ \AA})^{\beta}]$ , where  $\tau_{25}$  is the optical depth at 25 Å. Inspired by the behaviour of the total cross-section shown in Fig. 1 of Wilms et al. (2000), we choose  $\beta = 3$ ; it is intermediate between the steeper decrease of the cross-sections of Helium and Hydrogen at these energies and the shallower one for Carbon and Nitrogen. For the scaling, we use the relation given by Morrison & McGammon (1983),  $\tau_{25} = 7.6 \times 10^{-22} N_{\text{H}}$ .

The main systematic uncertainty in our correction is due to the relative abundances, in particular for Oxygen and for the lighter elements represented by  $\tau_{25}$  (see §5). The latter uncertainty could be quite large: for example, calculating  $\tau_{25}$  from the abundances and cross-

---

<sup>3</sup>The good match to the solar abundances is perhaps surprising, given the discrepant abundance ratios found in other recent X-ray spectroscopic studies (N. Schultz, 2005, personal comm.); it may be a consequence of the fact that AXPs are not affected by binary interactions.

Table 4. Inferred Hydrogen column densities and amounts of visual extinction

AXP	$N_{\text{H}}(\text{O K})$	$N_{\text{H}}(\text{Ne K})$	$N_{\text{H}}(\text{Mg K})$	$\langle N_{\text{H}} \rangle$	$A_V$
<i>Abundance<sup>a</sup></i>	$4.6 \times 10^{-4}$	$6.9 \times 10^{-5}$	$3.4 \times 10^{-5}$		
4U 0142+61	$0.60 \pm 0.09$	$0.77 \pm 0.19$	$0.65 \pm 0.15$	$0.64 \pm 0.07$	$3.5 \pm 0.4$
1E 2259+586	...	$1.23 \pm 0.58$	$1.06 \pm 0.41$	$1.12 \pm 0.33$	$6.3 \pm 1.8$
1E 1048.1–5937	...	$1.0 \pm 1.0$	$0.8 \pm 0.7$	$0.87 \pm 0.57$	$4.9 \pm 3.2$
1RXS J170849.0–400910	...	$2.1 \pm 0.7$	$0.9 \pm 0.6$	$1.4 \pm 0.4$	$7.7 \pm 2.2$

Note. — All column densities  $N_{\text{H}}$  are in units of  $10^{22} \text{ cm}^{-2}$ . Column  $\langle N_{\text{H}} \rangle$  is the weighted mean of all measurements. For previous determinations of the hydrogen column density, from broad-band spectral fits, see Table 1.  $A_V$  is the extinction (in magnitudes) in the  $V$ -band; the errors listed are statistical only, and do not include systematic uncertainties in the conversion from  $N_{\text{H}}$ . The  $N_{\text{H}}$  values themselves do not include several possible systematic errors (see §6).

<sup>a</sup>Elemental abundance  $N_{\text{O,Ne,Mg}}/N_{\text{H}}$  used to convert from the measured column from Table 3 to the equivalent Hydrogen column listed here. See §3 and 5 for details.

sections in Morrison & McCammon (1983), one gets a correction  $\sim 1.7$  times larger – and thus 1.7 times larger implied intrinsic flux – than by using those in Wilms et al. (2000). This discrepancy, however, reduces rapidly with decreasing wavelength, and does not alter the shape of the spectra by much (at least on the logarithmic scale on which they are shown).

In Fig. 2, we show the observed (circles) and de-extincted (triangles) spectrum of 4U0142+61: all the edges apparent in the observed spectrum have been removed in the corrected spectrum (though discrete features are still evident, such as those due to the multiple edges of iron at 17.5 Å). From the de-extincted points, it is clear that the de-extincted spectrum falls with wavelength at longer wavelengths.

In order to see how it might have been possible to infer a rise at longer wavelengths from broad-band data, we also show the spectrum de-extincted with  $N_{\text{H}} = 9.5 \times 10^{21} \text{ cm}^{-2}$  (crosses), as found by White et al. (1996) from *ASCA* data, and overdraw their fit of the sum of a power-law and black-body (upper curve) and this same model extinguished by their value of the hydrogen column (lower curve).<sup>4</sup> One sees from the Figure that, qualitatively, their fit is not unreasonable, so the source has not varied much. Looking in detail, however, especially near the Oxygen edge, it is clear that their column density is too high, and that the data are inconsistent with a intrinsic spectrum rising at long wavelengths.

In Fig 3, we show the de-extincted spectra derived for all four AXPs under consideration. Two things are immediately apparent: they are not consistent in shape with one-another, and there is no continuation at low energies of any power-law component representing the emission at  $> 2 \text{ keV}$ : the photon indices, measured from power-law plus black-body fits, of 2.4 to 4.0 correspond to slopes of  $\alpha = -0.6, -0.1, 0.4$ , and 1.0 ( $F_{\lambda} \propto \lambda^{\alpha}$ ), for 1RXS J170849.0–400910, 1E 1048.1–5937, 4U 0142+61, and 1E 2259+586, respectively, while the spectra shown have indices of approximately  $\alpha = -3, -2, -2$ , and 0 (if the low-energy tail is taken to be a power-law). Note that the largest cause of uncertainty in these derived spectra are the uncertainties in the column depths of the individual edges, rather than abundances, detector response or photon statistics. However, the conclusion that any power-law component at short wavelengths does not continue to long wavelength is robust.

The above result raises a paradox: How can it be that even for the sources other than 4U 0142+61, for which the equivalent hydrogen columns  $N_{\text{H}}$  we determine are consistent with those from power-law plus black-body fits, we do not see the power-law component at long wavelength? The answer lies in the fact that the low-energy region is actually not reproduced all that well in typical fits to broad-band spectra, but this may not be noticed in

---

<sup>4</sup>White et al. (1996) used the cross-sections of Morrison & McCammon (1983) in calculating extinction, so we have used this also in this instance only, for consistency.

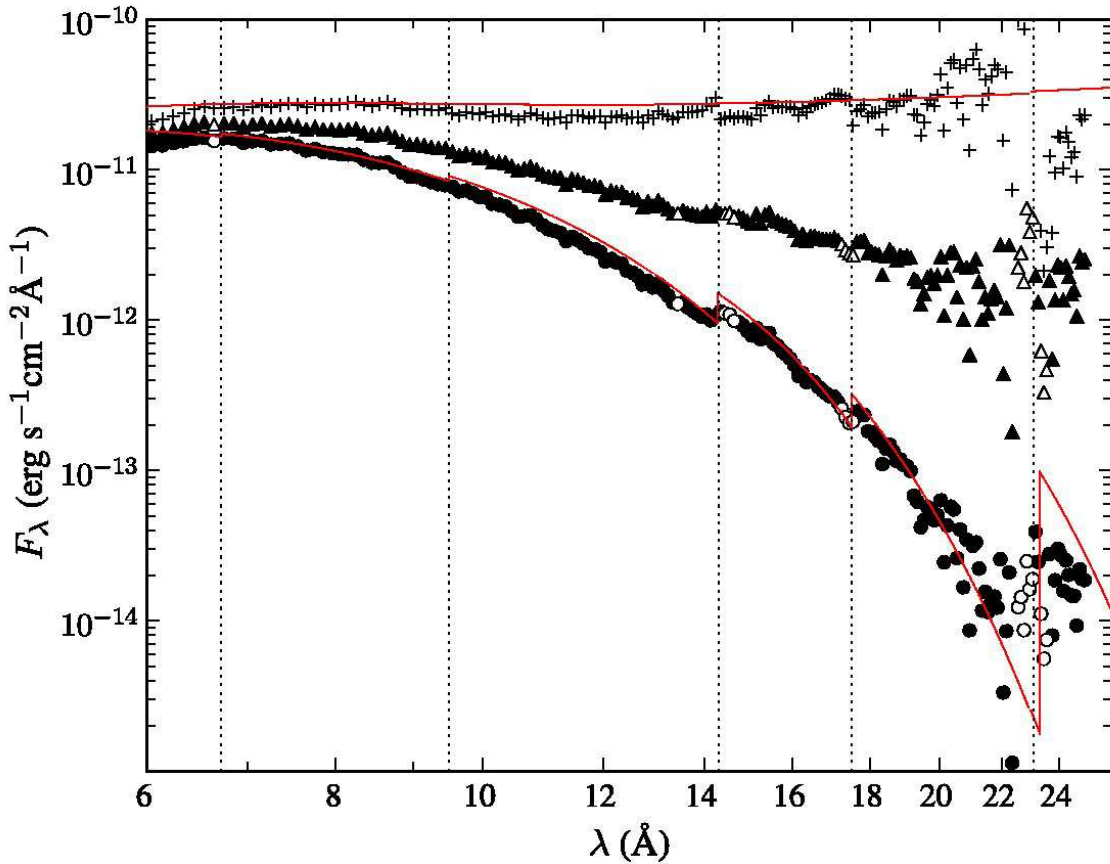


Fig. 2.— Spectra of 4U 0142+61 as observed (circles), de-extincted with the  $N_{\text{H}}$  found in this work and the abundances as described in the text (triangles) and de-extincted using Morrison & McCammon’s cross-sections and  $N_{\text{H}} = 9.5 \times 10^{21} \text{ cm}^{-2}$  (crosses). Open symbols indicate points affected by lines and other structure near the different edges. The over-drawn solid lines are the models of White et al. (1996) that best fit their broad-band *ASCA* data (see text). Vertical lines show the locations of the Si-K, Mg-K, Ne-K, Fe-L, and O-K photo-electric absorption edges.

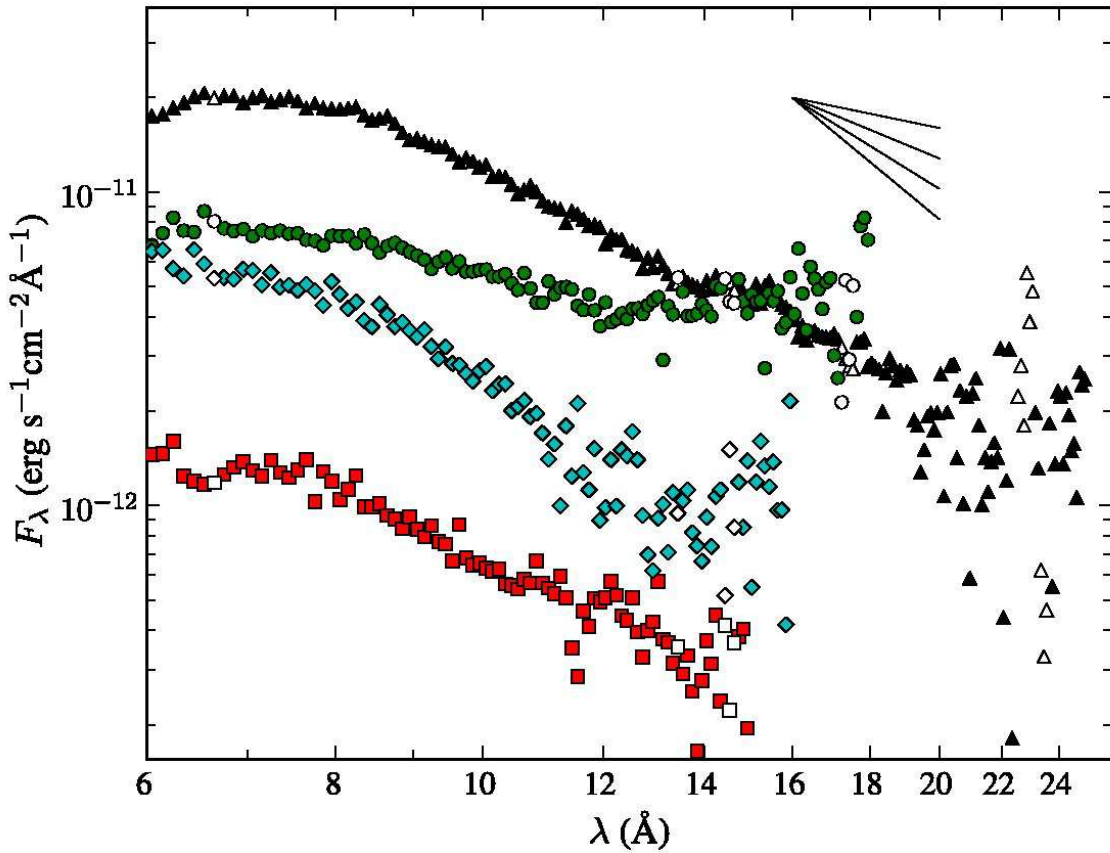


Fig. 3.— Spectra for each AXP, de-extincted with the column densities and continuum extinction found in the text. Black triangles are 4U 0142+61, green circles 1E 2259+586, red squares 1E 1048.1–5937, and cyan diamonds 1RXS J170849.0–400910. Open symbols are affected by absorption edge structure and absorption lines (see text). The spectra have been truncated where the signal-to-noise ratio per bin decreases below about 1. Also shown are power laws ( $F_\lambda \propto \lambda^\alpha$ ,  $\alpha = -1, -2, -3, -4$ ) to guide the eye.

the formal  $\chi^2$  since it has relatively few counts and thus carries little weight (if it is included at all). For a good example of this, see Fig. 2 in Woods et al. (2004): below 0.75 keV, the data lie systematically  $\sim 20\%$  above the model (particularly easy to see in this figure, since it has a panel with the ratio of the data to the model, rather than the usual, less instructive  $\chi$  residuals). With relatively few counts and larger uncertainties, these points do not affect much the overall  $\chi^2$ , but clearly (by eye) they are not well described by the model (and indeed a bad fit would likely have been found if the data had been binned more heavily).

While at low energies there is no evidence of continuations of high-energy power-law components, the spectra also do not decline as fast as would be expected if they were due to a black-body component. If the thermal emission arises from the neutron-star surface, as seems likely, this might simply reflect a range of temperatures on the surface. Alternatively, it may indicate that more realistic models are required to describe the emission, which also include the effects of magnetic field, interactions with high-energy particles in the magnetosphere, and gravitational light-bending (the latter particularly important for phase-resolved spectra).

Finally, looking in detail at the spectra, it appears that for 4U 0142+61, there is a hint of a feature in the spectrum at about 13.5 Å (this is easier to see in Fig. 4 at around  $2 \times 10^{17}$  Hz). One could interpret this either as a broad absorption feature at  $\sim 13.5$  Å, or a broad emission feature at  $\sim 15$  Å. Assuming it is cyclotron absorption (emission), i.e.,  $E_{cyc} = \hbar e B / mc$ , this corresponds to  $7.9 \times 10^{10}$  G ( $7.1 \times 10^{10}$  G) for electrons or  $1.5 \times 10^{14}$  G ( $1.3 \times 10^{14}$  G) for protons. If the line is red-shifted, the inferred magnetic field strength would increase by a factor  $1 + z_{GR} = (1 - 2GM/Rc^2)^{-1/2}$ , equal to  $\sim 1.3$  at the surface (for a neutron star with  $M = 1.4 M_\odot$  and  $R = 10$  km). Intriguingly, the value for proton cyclotron lines is close to the magnetic dipole field strength inferred from timing measurements,  $B_{\text{dip}} = 3.2 \times 10^{19} \sqrt{P \dot{P}} = 1.3 \times 10^{14}$  G (Woods & Thompson 2004).

## 7. Optical extinction

Our revised X-ray extinction measurements also allow us to estimate the extinction in the optical and infrared. For this purpose, we use the relation between the Hydrogen column  $N_H$  and visual extinction  $A_V$  derived by Predehl & Schmitt (1995):  $A_V = 5.6(N_H/10^{22} \text{ cm}^{-2})$  mag. The resulting values of  $A_V$  are listed in Table 4. Here, the errors on  $A_V$  listed are statistical, i.e., they do not include the uncertainty in the conversion factor. The latter uncertainty could be fairly large, both because there is substantial scatter in the measurements used by Predehl & Schmitt, and because their sample had typically lower values of extinction. Furthermore, their hydrogen column is not measured directly, but is based on X-ray extinction measurements and thus a measure of elements which contribute

significantly to absorption in X-rays, i.e., Carbon, Oxygen, Neon, and Magnesium. The latter should not be a problem in our case, however, since we measure some of the same elements in Predehl & Schmitt’s sensitivity range (they did not have the spectral resolution to measure individual absorption edges), and thus systematic effects in converting to  $N_{\text{H}}$  should cancel. The only caveat is that we used the revised solar abundances of Asplund et al. (2004), while Predehl & Schmitt used, implicitly, the old solar abundances. For Neon and Magnesium, however, the abundances have not changed, while the change for Oxygen should not have a large effect, since for the one case where we measure it – for 4U 0142+61 only – the inferred  $N_{\text{H}}$  is consistent with the values inferred from Neon and Magnesium (see Table 4).

While the above indicates one should be somewhat careful in using the absolute values of the reddening, the relative reddenings should be much more accurate, since any systematic uncertainties in the conversion should be similar from source to source. Our results indicate that in order of increasing reddening, the AXPs are 4U 0142+61, 1E 1048.1–5937, 1E 2259+586 and 1RXS J170849.0–400910.

We can compare our revised estimates with earlier work. First, for 4U 0142+61, Hulleman et al. (2004) found from the colors of field stars, that the reddening along the line of sight was likely substantially lower than the value  $A_V = 5.1$  inferred from the literature values of  $N_{\text{H}}$  for the power-law plus black-body model. Our new value of  $A_V = 3.5 \pm 0.4$  is consistent with the range of  $A_V = 2$  to 4 seen in their Fig. 3. Second, comparing 4U 0142+61 with 1E 1048.1–5937, Durant & van Kerkwijk (2005) noted that in order for the broad-band optical/infrared spectrum of these AXPs to have the same shape, the difference in reddening would have to be  $\Delta A_V = 2.5 \pm 0.5$ . This was inconsistent with previous estimates, which gave very similar values of  $A_V$  (based on the very similar values of  $N_{\text{H}}$ ; see Table 1), but is consistent with our new results, which give a difference in reddening of  $\Delta A_V = 1.3 \pm 3$ . Thus, the optical/infrared spectra of the different AXPs may be similar in shape, and therefore produced by the same mechanism.

## 8. The Spectral Energy Distribution of 4U 0142+61

With our empirical estimates of the intrinsic (soft) X-ray spectra, and the revised estimate for optical/infrared reddening, we can re-examine the spectral energy distributions of the AXPs. We only consider 4U 0142+61, since this object is the only one for which we find a significantly different column density from that typically quoted. Furthermore, it has the best X-ray data, and the best broad-band coverage, from mid-infrared (Wang et al. 2006), to near-infrared and optical (Hulleman et al. 2004; Israel et al. 2004), to hard X-rays (Den

Hartog et al. 2006).

Figure 4 shows the inferred intrinsic spectral energy distribution of 4U 0142+61, determined with our new values of  $N_{\text{H}}$  and  $A_V$ . The interpretation of the optical and infrared emission is still unclear: it could be understood as combination of a large mid-infrared bump combined with a rising power-law that has a sharp break at B, or as a combination of a much smaller mid-infrared bump combined with a flatter power-law and a large emission feature centered between R and V. Wang et al. (2006) interpret the mid-infrared bump as arising from a passively illuminated dusty disc. This disc is presumably formed from supernova fall-back material, and the data is well fitted by a blackbody from dust at the sublimation radius. This disc would also influence the flux in the K-band. Wang et al. used our new estimate of  $N_{\text{H}}$ , but their results are not very sensitive to the exact value of  $N_{\text{H}}$ , as long as the reddening is above  $A_V \approx 2.6$  (Chakrabarty, 2005, pers. comm.).

The soft X-ray spectrum in Figure 4 suggestively has a slope which would meet up with the optical points if extended. This is in marked contrast with the earlier power-law models, which grossly over-predict the optical emission (see §1). The uncertainty in the slope of the soft X-rays is dominated by the uncertainty in the Hydrogen column (and its systematics, particularly due to abundance uncertainties), so there is not enough information at present to say whether the break between the B- and V-bands is due to an emission or an absorption feature.

## 9. Conclusions

We have attempted to measure the extinction to the AXPs without making assumptions about what their intrinsic spectral shapes might be. With our resulting best estimates, we derived intrinsic spectra, which can be compared with each other as well as with predictions, such as those from simulations and semi-analytic models that are now being produced within the magnetar framework (e.g., Lyutikov & Gavriil 2006; R. Fernández & C. Thompson 2006, pers. comm.).

Apart from these comparisons, future work could include extending our analysis to other sources (once better spectra become available), or improving the precision of our measurements using further *XMM-Newton* observations (some already taken but not yet public) or *Chandra* spectra (some available). More interestingly, by measuring the run of reddening with distance along the line of sight to the AXPs (using field stars), our extinction estimates can be used to estimate distances and thus determine the intrinsic luminosities of the AXPs. It turns out that although the extinctions are not very well determined, the

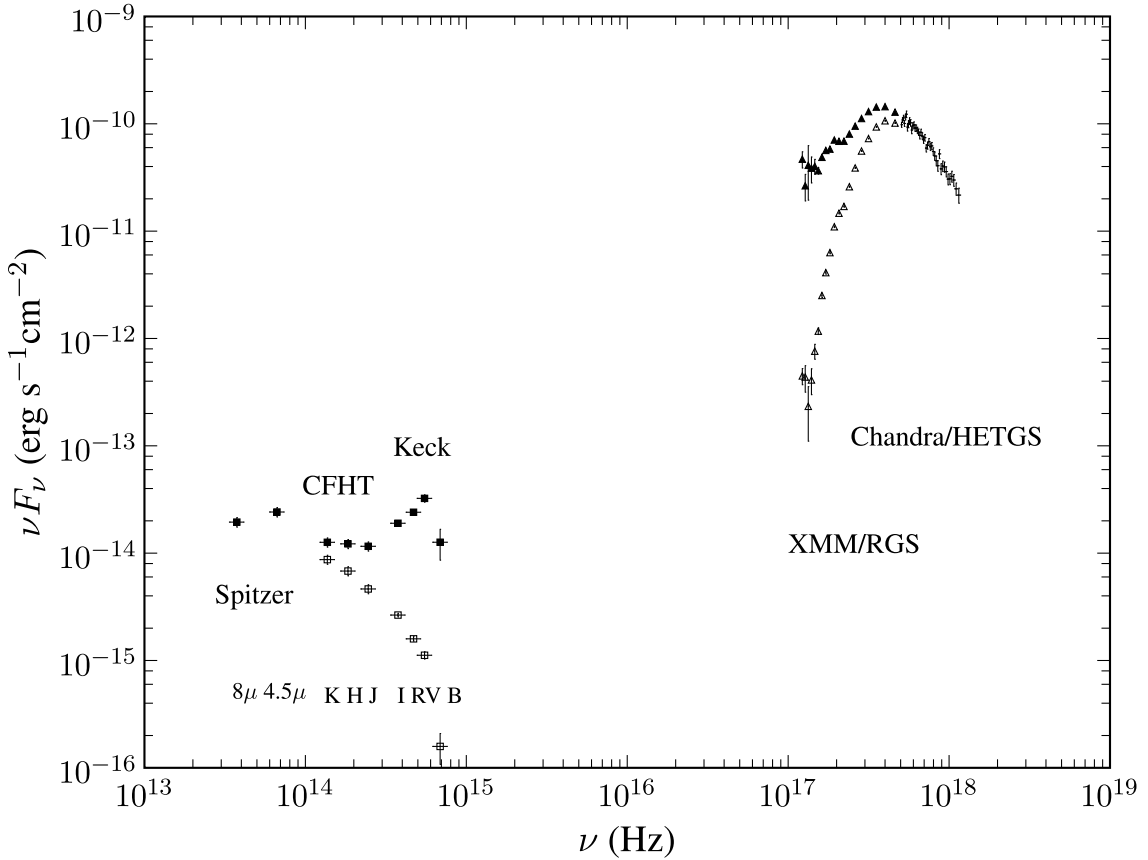


Fig. 4.— Spectral energy distribution for 4U 0142+61. Triangles are XMM/RGS data, as observed (open) and de-extincted (filled) as described in the text. Open squares are observed broad-band photometry (mid-IR from Wang et al., 2006; JKH from Israel et al. (2004); BVRI from Hulleman et al., 2004). Filled squares are the photometric points de-reddened with  $A_V = 3.5$  (see text). Crosses in the higher-energy X-ray part of the spectrum come from *Chandra* (Juett et al., 2002); extinction is not important in this region of the spectrum. XMM data is binned in frequency ( $\delta\nu$ ) corresponding to  $\delta\lambda = 1 \text{ \AA}$ , and *Chandra* data to  $\delta\lambda = 0.1 \text{ \AA}$  for clarity.

AXPs fall into areas of rapidly rising extinction associated with spiral arms, and so can be well localized (Durant & Van Kerkwijk, 2006). Finally, our reddening estimates will place on much firmer footing inferences from further optical and infrared studies, such as could be used, e.g., to uncover the nature of the break seen between  $V$  and  $B$  in 4U 0142+61 (Hulleman et al. 2004) or to measure the precise parameters of the possible debris disk around that source (Wang et al. 2006).

We thank Adrienne Juett, Norbet Schultz, and Hermann Marshall for discussion of the X-ray absorption edges, and Vik Dhillon for letting us use his *XMM-Newton* data on 1E 1048.1–5937 before it became public. We also gratefully acknowledge the comments of the anonymous referees, which helped us clarify the statistical significance of our analysis and the presentation of our results. This work is based on archival observations obtained with XMM-Newton, an ESA science mission, and made extensive use of NASA’s ADS and Simbad. We acknowledge financial support from NSERC.

## REFERENCES

Anders, E., Grevesse, N., 1989, *Geochimica et Cosmochimica Acta*, 53, 197

Asplund, M., Grevesse, N., Jacques Sauval, A., 2004, in *Cosmic Abundances as Records of Stellar Evolution and Nucleosynthesis*, ASP Conference Series, eds F. N. Bash and T. G. Barnes

Bahcall, J. N., Basu, S., Serenelli, A. M., 2005, *ApJ*, 631, 1281

Balucinska-Church, M., McCammon, D., 1992, *ApJ*, 400, 699

den Hartog, P., Hermsen, W., Kuiper, L., Vink, J., int Zand, J., & Collmar, W., 2006, *A&A*, accepted, see [astro-ph/0601644](#)

den Herder, J., et al., 2001, *A&A*, 365, L7

Drake, J., Testa, P., 2005, *Nature*, 436, 525

Durant, M., & van Kerkwijk, M., 2005, *ApJ*, 627, 376

Durant, M., & van Kerkwijk, M., 2006, *ApJ*, accepted ([astro-ph/0606027](#))

Göhler, E., Staubert, R., Wilms, J., 2004, *MmSAI*, 75, 464

Gould, R. J., Jung, Y., 1991, *ApJ*, 373, 271

Ho, W., Lai, D., 2003, MNRAS, 338, 233

Hulleman, F., van Kerkwijk, M., & Kulkarni, S., 2000, Nature, 408, 689

Hulleman, F., Tennant, A., van Kerkwijk, M., Kulkarni, S., Kouveliotou, C., Patel, S., 2001, ApJ, 563, L49

Hulleman, F., van Kerkwijk, M., & Kulkarni, S., 2004, A&A, 416, 1037

Israel, G., Stella, L., Covino, S., Campana, S., Angelini, L., Mignani, R., Mereghetti, S., Marconi, G., Perna, R., 2004, IAU Symposium no. 218

Jensen, G., 1999, Bulletin of the American Astronomical Society, 32, 724

Juett, A., Marshall, H., Chakrabarty, D., Schulz, N., 2002, ApJ, 568, L31

Juett, A. M., Schulz, N. S., Chakrabarty, D., Canizares, C. R., 2003, AAS HEAD meeting 7, 06.02

Juett et al, 2006, in preparation

Kuiper, L., Hermsen, W., Mendez, M., 2004, ApJ, 613, 1173

Lodders, K., 2003, ApJ, 591, 1220

Lyutikov, M., & Gavriil, F., 2006, MNRAS, 368, 690

Matteucci, F., Chiappini, C., 2005, PASA, 22, 49

Morrison, R., McCammon, D., 1983, ApJ, 270, 119

Oosterbroek, T., Parmar, A., Mereghetti, S., Israel, G. L., 1998, A&A, 334, 925

Patel, S., Kouveliotou, C., Woods, P., Tennant, A., Weisskopf, M., Finger, M., Göğüş, E., van der Klis, M., Belloni, T., 2001, ApJ, 563, L45

Predehl, P., & Schmitt, J., 1995, A&A, 293, 889

Press, W., Teukolsky, S. A., Vetterling, W., and Flannery, B., 1992, *Numerical Recipes: the art of scientific computing* 2nd Edition, Cambridge University Press

Rea, N., Israel, G. L., Stella, L., Oosterbroek, T., Mereghetti, S., Angelini, L., Campana, S., Covino, S., 2003, ApJ, 586, L65

Rea, N., Oosterbroek, T., Zane, S., Turolla, R., Méndez, M., Israel, G. L., Stella, L., Haberl, F., 2005, MNRAS, 361, 710

Rho, J., Petre, R., 1997, *ApJ*, 484, 828

Schmelz, J., Nasraoui, K., Roames, J., Lippner, L., Garst, J., 2005, *ApJ*, 634, L197

Strüder, L., et al., 2001, *A&A*, 365, L18

Takei, Y., Fujimoto, R., Mitsuda, K., Onaka, T., 2002, *ApJ*, 581, 307

Tiengo, A., Mereghetti, S., Turolla, R., Zane, S., Rea, N., Stella, L., Israel, G. L., 2005, *A&A*, 437, 997

Turner, M., et al., 2001, *A&A*, 365, L27

Ueda, Y., Mitsuda, K., Murakami, H., Matsushita, K., 2005, *ApJ*, 620, 274

Wang, Z., Chakrabarty, D., Kaplan, D., 2006, *Nature*, 440, 772

Weisskopf, M., O'Dell, S., Paerels, F., Elsner, R., Becker, W., Tennant, A., Swartz, D., 2004, *ApJ*, 601, 1050

Werner, D., & Yakovlev, D., 1995, *A&AS*, 109, 125

White, N. E., Angelini, L., Ebisawa, K., Tanaka, Y., Ghosh, P., 1996, *ApJ*, 463, L83

Wilms, J.; Allen, A.; McCray, R., 2000, *ApJ*, 542, 914

Woods, P., & Thompson, C., 2004, in “Compact stellar X-ray sources”, eds Lewin, W., van der Klis, M.

Woods, P., Kaspi, V., Thompson, C., Gavriil, F., Marshall, H., Chakrabarty, D., Flanagan, K., Heyl, J., Hernquist, L., 2004, *ApJ*, 605, 378

Young, P., 2005, *A&A*, 444, L45

Zane, S., Turolla, R., Stella, L., Treves, A., 2001, *ApJ*, 560, 384